IEEE Access
Multidisciplinary | Rapid Review | Open Access Journal

Received 23 August 2023, accepted 6 September 2023, date of publication 11 September 2023,
date of current version 14 September 2023.

Digital Object Identifier 10.1109/ACCESS.2023.3313720

RESEARCH ARTICLE

Generalized Phase-Polarization Cancellation for Broadband Radar Cross-Section Reduction

MOHAMMAD SHIRMOHAMMADKARIMI[1], ALI GHADIMI[2], MOHAMMAD SOLEIMANI[1], AND VAHID NAYYERI[2], (Senior Member, IEEE)
[1]School of Electrical Engineering, Iran University of Science and Technology, Tehran 1684613114, Iran
[2]School of Advanced Technologies, Iran University of Science and Technology, Tehran 1684613114, Iran

Corresponding author: Vahid Nayyeri (nayyeri@iust.ac.ir)

ABSTRACT This study presents a novel approach to decrease the radar cross-section (RCS) by integrating and expanding the phase cancellation and polarization conversion methods. In this proposed technique, only one unit cell, akin to the polarization conversion method, is utilized. The RCS reduction surface is comprised of arrays of this unit cell; each array is rotated by 90 degrees in relation to its neighboring arrays. Unlike previous RCS reduction methods, which employed periodic arrangements of unit cells that either kept the polarization of the reflected wave unrotated or rotated it by 90 degrees, the proposed generalized method enables the unit cells to rotate the polarization of the reflected wave arbitrarily. This is achieved by eliminating the symmetry requirement in the unit cell design. The mathematical theory for the proposed RCS reduction method has been developed. To demonstrate the method's feasibility, a unit cell was designed using a pattern optimization method based on the pixelization of the cell surface, and a binary particle swarm optimization algorithm was employed as a proof of concept. A surface was formed by constructing 4×4 arrays of 7×7 designed unit cells, where each array was rotated 90 degrees relative to its side array. The measured results demonstrate a 10-dB monostatic RCS reduction bandwidth of 115%, from 2.8 GHz to 10.4 GHz, which is in excellent agreement with the bandwidth obtained using the developed theory.

INDEX TERMS Phase cancellation, polarization conversion, radar cross section reduction, binary optimization.

I. INTRODUCTION

In stealth technology, reducing the radar cross-section (RCS) of metal equipment is crucial. This can generally be accomplished by two approaches. First, an object is covered with a radar absorber, which converts electromagnetic energy into heat. Although there are undeniable benefits to using radar absorption coatings, there are significant downsides, such as their relatively high thickness and weight and their maintenance expenses. The second strategy is to deflect the reflected waves from the target. Previously, this was done by modifying the geometric structure of the target, which is not only costly but also has aerodynamic constraints and is not always practical.

Recently, another approach based on phase cancellation has been employed to scatter the reflected wave from the target. In this method, an artificial layer is put on the metal surface, causing the radiation wave to disperse. This approach was initially proposed by integrating the perfect magnetic conductor (PMC) and the perfect electrical conductor (PEC) tiles on a checkered surface [1]. The PMC tiles in this checkered structure return the wave in phase, while the PEC tiles reflect the wave out of phase, causing the reflected field from the whole surface to be canceled in the direction of the incident. Although the thinness and lightness of these surfaces had significant advantages, the narrow bandwidth of the radar cross-section reduction limited their application. To address this problem, in the following works, arrays of two artificial magnetic conductor (AMC) cells were utilized instead of PMC and PEC tiles to increase the phase cancellation bandwidth (i.e., the bandwidth wherein

The associate editor coordinating the review of this manuscript and approving it for publication was Bilal Khawaja.

the reflected waves from the two arrays (tiles) have a phase difference of about 180 degrees) [1], [2], [3], [4], [5], [6], [7], [8], [9], [10], [11], [12]. It should be noted that one of the considerations in designing the unit cell of this method is preserving a one-eighth (four axes) symmetry to make the surface insensitive to the polarization of the incident wave.

Utilizing polarization conversion surfaces is another recent method for deflecting the reflected wave from the targets leading to RCS reduction [13], [14], [15], [16], [17], [18]. In contrast to the phase cancellation approach, which employs two types of unit cells, this method uses only a single unit cell with a diagonal symmetry so that its array can spin the incident wave polarization 90 degrees. As indicated in FIGURE 1, four arrays of the cell are positioned next to each other after rotating 90 degrees with respect to the center. The reflected field from the whole surface shown in FIGURE 1 is the summation of the reflections from the four arrays, which cancel out each other two by two in the normal direction. It should be noted that in this approach, the bandwidth of the RCS reduction is determined and restricted by the bandwidth wherein the cells (in a period configuration) spin the polarization 90 degrees.

In other works, coding surfaces including several unit cells in an irregular formation (instead of the regular formation of the cells on the aforementioned RCS reducer surfaces based phase cancellation and polarization conversion methods) were used for RCS reduction [19], [20], [21], [22]. Different unit cells were designed to provide different reflection phases; then, the formation of the cells on the surface was optimized so that the reflections from the cells cancel each other. The drawback of this strategy is that the formation of the cells depends on the shape and dimensions of the underlying object; in other words, the covering surface should be designed again for different underlying objects.

In this paper, we present a novel technique for wideband-reducing RCS based on phase-polarization cancellation. This approach builds upon existing methods of phase-cancellation and polarization conversion and was briefly introduced in the authors' recent conference paper [23]. In this technique, a unit cell is designed and arranged in four arrays next to each other after rotating 90 degrees around the origin, as depicted in FIGURE 1, similar to the polarization conversion method. However, the design of the unit cell in the proposed method is more general than earlier approaches, which were based on maintaining the polarization of the reflected signal (in phase cancellation methods) or rotating it by 90 degrees (in polarization conversion method). The proposed method removes restrictions on both the symmetry of the unit cell and the rotation of wave polarization. A unit cell array can, therefore, arbitrarily rotate the incident wave polarization, increasing design flexibility and resulting in RCS reduction in a broader bandwidth. While our conference paper [23] presents only the main idea, here, we provide more detailed explanations and validation of this approach.

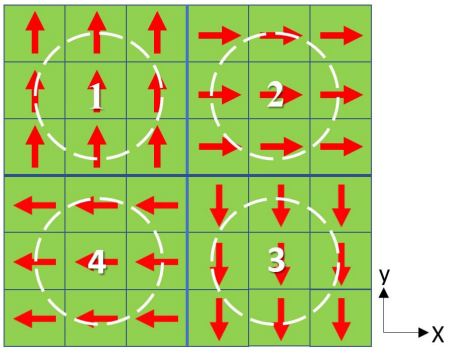

FIGURE 1. Building block of an RCS reducer surface comprising four arrays of a unit cell, each of which is rotated by 90 degrees with respect to the neighboring arrays.

To demonstrate the feasibility of our proposed approach, we have designed a unit cell using a pattern optimization method. This technique involves pixelating the surface of a unit cell and optimizing it using a binary (or ternary) optimization algorithm. The effectiveness of this method has been demonstrated in various applications such as radar cross-section reducer surfaces [7], [21], [24], high impedance surfaces [25], [26], electromagnetic energy harvesting surfaces [27], absorbers [28], sensors [29], decoupling elements between microstrip antennas [30], polarization converters [31], [32], and frequency-selective surfaces [33]. In our present study, we have utilized the pattern optimization method to design a unit cell for our proposed phase-polarization cancellation approach. The simulation and measurement results validate the effectiveness of our approach in achieving broadband RCS reduction.

II. THEORY OF GENERALIZED PHASE -POLARIZATION CANCELLATION

The objective of this study is to reduce the RCS utilizing a surface that incorporates rotated arrays of a unit cell. As illustrated in FIGURE 1, each array is rotated by 90 degrees relative to the neighboring arrays. In this section, we derive a general condition for a unit cell that, when arranged according to FIGURE 1, results in RCS reduction.

We begin our analysis by assuming that an electromagnetic wave that is linearly polarized in the y-direction is normally incident upon the structure depicted in FIGURE 1. The electric fields associated with the incident and reflected waves are expressed as follows:

$$\vec{E}^i = {E_y}^i \, \hat{a}_y \tag{1}$$

$$\vec{E}^r = \Gamma_{co} \, {E_y}^i \, \hat{a}_y + \Gamma_{cr} \, {E_y}^i \, \hat{a}_x \tag{2}$$

where Γ_{co} and Γ_{cr} are the co- and cross-polarized components (in the y- and x- directions) of the reflected electric field from the whole structure, respectively.

The reflected field $\vec{E}^r$ generated by the surface depicted in FIGURE 1 is the sum of the reflected fields of each individual

array and can be written as

$$\vec{E}^r = \frac{1}{4}\sum_{j=1}^{4}\left(\vec{E}^r\right)_j, \tag{3}$$

where j represents the index assigned to each array depicted in FIGURE 1. It should be noted that all unit cells within a given array have the same orientation. As a unit cell is not bound by any symmetry, the polarization vector of the reflected wave from an array can rotate arbitrarily relative to that of the incident wave. Consequently, the reflected electric field of the j^{th} array can be expressed as follows:

$$\left(\vec{E}^r\right)_j = \left(\Gamma_{yy}\right)_j E_y{}^i\,\hat{a}_y + \left(\Gamma_{xy}\right)_j E_y{}^i\,\hat{a}_x \tag{4}$$

where $\left(\Gamma_{yy}\right)_j$ and $\left(\Gamma_{xy}\right)_j$ respectively represent the y- and x-components of the reflection coefficient from the j^{th} array excited by a y-polarized incident wave. Comparing (2) and (3), we have:

$$\Gamma_{co} = \frac{1}{4}\sum_{j=1}^{4}\left(\Gamma_{yy}\right)_j \tag{5a}$$

$$\Gamma_{cr} = \frac{1}{4}\sum_{j=1}^{4}\left(\Gamma_{xy}\right)_j \tag{5b}$$

Given that the four arrays comprising the RCS reducer surface are identical and only differ in their relative rotation, the components of the reflection coefficient from these arrays are not independent. However, as the arrays (not the unit cells) possess rotational symmetry, certain relationships exist between the components of reflection coefficients of the arrays, as outlined below:

$$\left(\Gamma_{yy}\right)_3 = \left(\Gamma_{yy}\right)_1 \tag{6a}$$

$$\left(\Gamma_{xy}\right)_3 = \left(\Gamma_{xy}\right)_1 \tag{6b}$$

$$\left(\Gamma_{yy}\right)_2 = \left(\Gamma_{yy}\right)_4 = \left(\Gamma_{xx}\right)_1 \tag{6c}$$

$$\left(\Gamma_{xy}\right)_2 = \left(\Gamma_{xy}\right)_4 = -\left(\Gamma_{xy}\right)_1 \tag{6d}$$

Equations (6b) and (6d) above utilize the principle of reciprocity, i.e., $\left(\Gamma_{xy}\right)_j = \left(\Gamma_{yx}\right)_j$. Upon substituting equation (6) into equation (5), we obtain the following expression:

$$\Gamma_{co} = \frac{1}{2}\left[\left(\Gamma_{yy}\right)_1 + \left(\Gamma_{xx}\right)_1\right] \tag{7a}$$

$$\Gamma_{cr} = 0 \tag{7b}$$

The reflected electric field from the entirety of the structure depicted in FIGURE 1 can be expressed as follows:

$$\vec{E}^r = \Gamma_{co}\, E_y{}^i\,\hat{a}_y \tag{8}$$

It is observed that the polarization of the reflected wave mirrors that of the incident wave, which can be attributed to the rotational symmetry of the overall structure depicted in FIGURE 1. It is worth mentioning that our full-wave simulations verify that the reflection from a structure, as shown in FIGURE 1, has a negligible cross-polarized component.

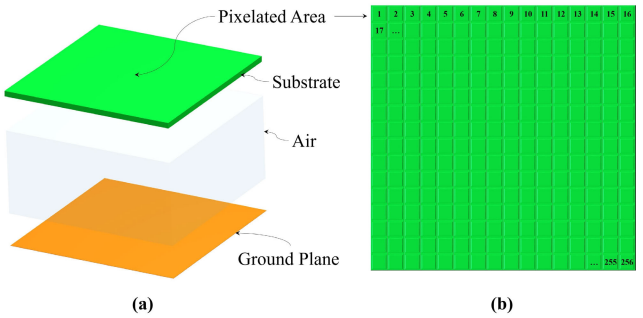

FIGURE 2. The unit cell before designing the metallic pattern: (a) 3D view, (b) top view of the pixelated surface of the unit cell (pixels' numbering is specified in (b)).

Based on equations (7a) and (8), it is evident that designing the unit cell to possess a small $\left|\left(\Gamma_{yy}\right)_1 + \left(\Gamma_{xx}\right)_1\right|$ results in a modest intensity of the reflected field from the structure, thereby accomplishing the objective of RCS reduction. Here, $\left(\Gamma_{xx}\right)_1$ and $\left(\Gamma_{yy}\right)_1$ refer to the co-polarized reflection coefficients of an array with the unit cells oriented in the same direction, under x-polarized and y-polarized radiation, respectively. According to equation (8), the relative RCS reduction (with respect to the total reflection, i.e., Γ=1) can be expressed as:

$$\text{RCS Reduction} = 20\,\log|\Gamma_{co}| = \Gamma_{co}\,[\text{dB}] \tag{9}$$

Thus, to achieve a reduction greater than 10 dB in RCS, the unit cell must be designed to satisfy the following condition within the desired frequency range:

$$20\log\frac{\left|\left(\Gamma_{yy}\right)_1 + \left(\Gamma_{xx}\right)_1\right|}{2} \le -10 \tag{10a}$$

or equivalently,

$$\left|\left(\Gamma_{yy}\right)_1 + \left(\Gamma_{xx}\right)_1\right| \le 0.63 \tag{10b}$$

It is worth noting that while the incident wave's polarization is assumed to be in the y-direction in the above analysis, the same holds true for an x-polarized incident wave, owing to the symmetry present in the overall structure depicted in FIGURE 1. In other words, the RCS of the overall structure is independent of the incident wave's polarization.

It is noticeable that in previous works using the polarization conversion technique [13], [14], [15], [16], [17], [18], the unit cell was supposed to have a diagonal symmetry so that $\Gamma_{xx} = \Gamma_{yy}$. In that case, (7a) is reduced to $\Gamma_{co} = \Gamma_{xx} = \Gamma_{yy}$. Consequently, the criterion for RCS reduction was to minimize the co-polarization reflection from the unit cell (in a periodic arrangement), i.e., $|\Gamma_{xx}|$. Therefore, in their works, the RCS reduction was achieved in the frequency band in which the co-polarized reflection from the unit cell (i.e., $\Gamma_{xx} = \Gamma_{yy}$) is almost zero, in other words, where the unit cell rotates the wave polarization around 90 degrees.

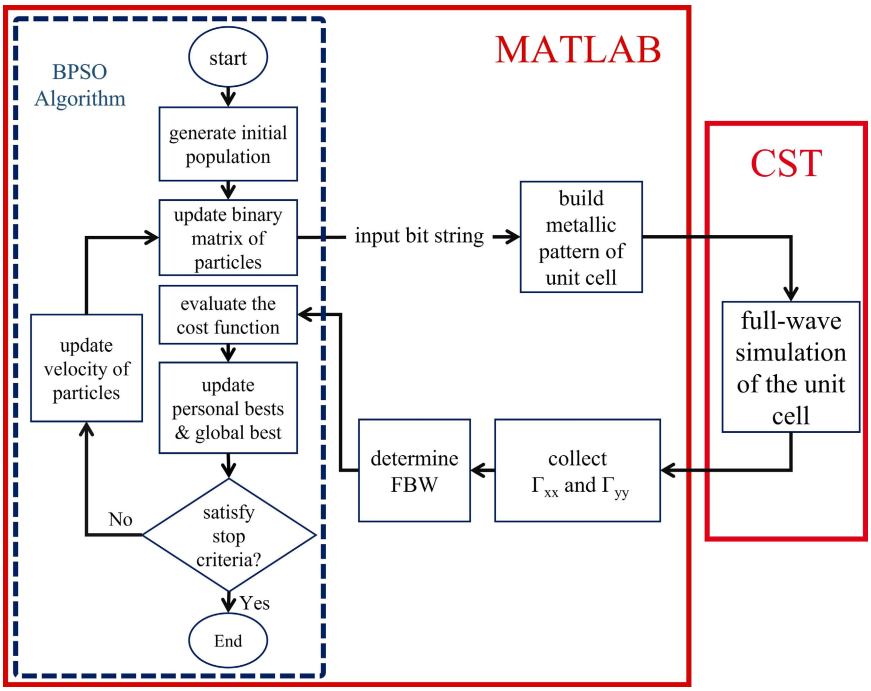

FIGURE 3. Flowchart of the pattern optimization process including a BPSO algorithm.

III. UNIT CELL DESIGN

An automated design method is employed to construct a unit cell that satisfies the criterion specified in equation (10) over a wide frequency range within a periodic array. This approach involves partitioning the surface of a unit cell into tiny pixels and assigning one bit to each pixel, with each bit taking on one of two values: 1 or 0, representing metal (copper) coverage and non-coverage of the associated pixel's surface, respectively. To determine the optimal value of each bit to achieve the desired goal, a binary optimization algorithm is utilized, specifically the binary form of the particle swarm optimization (PSO) algorithm known as BPSO.

The operating frequency limit is considered to be a few GHz due to the available measurement equipment. Based on previous works in this frequency range, a unit cell with dimensions of 16×16 mm^2 is selected and divided into 256 pixels of size 1×1 mm^2. It is important to note that increasing the number of pixels (reducing their size) allows for a more intricate unit cell design, but also results in an increased number of optimization variables, which can make optimization convergence more challenging. The substrate is a low-cost FR4 with a dielectric constant of 4.3, a loss tangent of 0.025, and a thickness of 0.5 mm. The substrate is backed by a ground (metal) plane with an air gap of 7.6 mm between them. A schematic of the unit cell with its pixelated surface is shown in FIGURE 2.

The BPSO algorithm is utilized to optimize the binary values of the bits. A population (swarm) of candidate solutions (each solution is referred to as a particle in this algorithm) searches the solution space to achieve optimization goals. Each particle adjusts its velocity based on its own best experience as well as the best global experience of the swarm, using a simple formula presented in [34], [35], [36], and [37].

FIGURE 3 illustrates the process of optimizing the metal pattern of the unit cell. The BPSO algorithm is implemented in MATLAB, and a link is established between MATLAB and CST Microwave Studio, a full-wave electromagnetic simulator. In this process, a random initial population is created in MATLAB, and the population bit strings are translated into related patterns, with the unit cells subsequently built in CST. Full-wave simulations are conducted in CST by applying periodic boundary conditions in the x and y directions, and Γ_{xx} and Γ_{yy} are obtained. From equations (7a) and (9), Γ_{co} and RCS reduction are then calculated from 2 GHz to 12 GHz.

The optimal number of particles for a BPSO algorithm depends on various factors, such as the problem's complexity, the number of optimization parameters, and available computational resources. A larger population size can improve the optimization algorithm's performance, but it also increases the computational cost. Typically, binary PSO uses a population size ranging from tens to hundreds of particles. There is no fixed rule for determining the optimal population size, but a common approach is to start with a small population and gradually increase it until achieving the desired level of convergence. For problems with not too many optimization parameters, a reasonable starting point is a population size of 50 to 100 particles. A general rule of thumb is also to use a population size of 10-20 times the number of dimensions [36], [38]. In our problem, we have 256 optimization parameters, which is a substantial number.

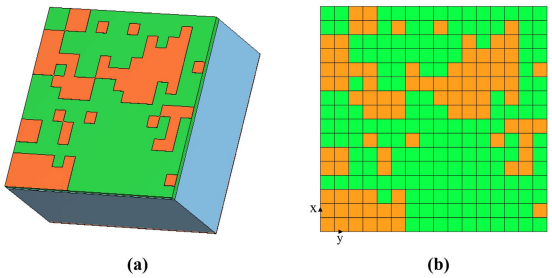

FIGURE 4. The outcome of the pattern optimization process: the (a) 3D view and (b) top view of the unit cell.

Additionally, as shown in FIGURE 3, every solution requires a full-wave simulation of the unit cell in CST, which takes a few minutes to complete on a desktop computer equipped with an 11th-generation Intel Core i7 processor. Given these computational constraints, it was not feasible to consider a very large population, i.e., several times the number of optimization parameters. Therefore, we chose a population size of 100 particles for our algorithm.

The objective is to maximize the fractional bandwidth of the RCS reduction, which is defined as the bandwidth at which the RCS reduction exceeds 10 dB. In the optimization process, after determining the value of RCS reduction, the low and high frequencies of the largest interval in which the RCS reduction is higher than 10 dB are extracted and designated as $fmin$ and $fmax$, respectively. The fractional bandwidth of RCS reduction is then computed as,

$$\text{FBW} = 2\frac{f_{max} - f_{min}}{f_{max} + f_{min}} \tag{11}$$

The optimization cost function is defined as the inverse of the fractional bandwidth, with the objective of minimizing it during the optimization procedure.

The optimization procedure with a population of 50 particles converged after several hundred iterations, resulting in the unit cell shown in FIGURE 4. The amplitudes and phases of Γ_{xx} and Γ_{yy} are presented in FIGURE 5, revealing that their values are not equal due to the unit cell's asymmetrical shape. It is noteworthy that if we assume zero loss in the structure, we would have $|\Gamma_{xx}|^2 + |\Gamma_{yx}|^2 = 1$ and $|\Gamma_{yy}|^2 + |\Gamma_{xy}|^2 = 1$, along with the theory of reciprocity, i.e., $\Gamma_{xy} = \Gamma_{yx}$, resulting in $|\Gamma_{xx}| = |\Gamma_{yy}|$. However, considering the low loss in the structure, we observe that $|\Gamma_{xx}|$ and $|\Gamma_{yy}|$ are not equal, as shown in FIGURE 5(a). Nonetheless, for relatively small losses, we can assume that $|\Gamma_{xx}| \approx |\Gamma_{yy}|$.

Considering a structure composed of four arrays of the designed unit cell that are rotated 90 degrees with respect to each other, the reflection coefficient of the overall structure is obtained from equation (7a) and plotted in FIGURE 6. It is important to note that this diagram also represents the RCS reduction according to equation (9). However, the value of the reflection coefficient (and hence the RCS reduction) depicted in FIGURE 6 is not the outcome of a full-wave

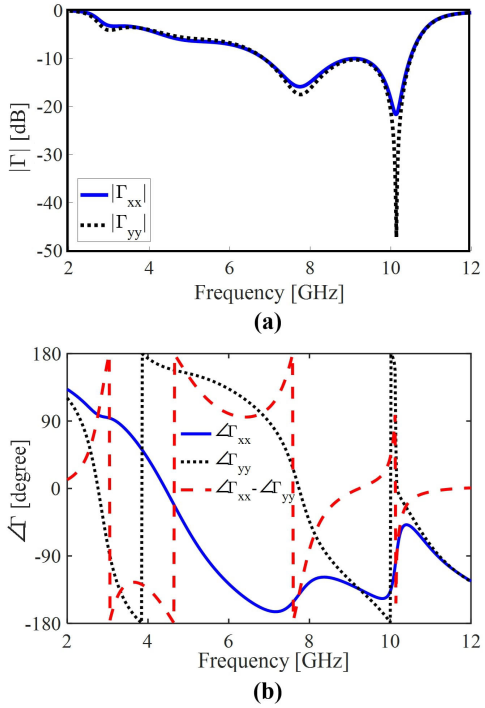

FIGURE 5. The (a) amplitude and (b) phase of Γ_{xx} and Γ_{yy} for the optimized unit cell (in a periodic configuration) depicted in FIGURE 4.

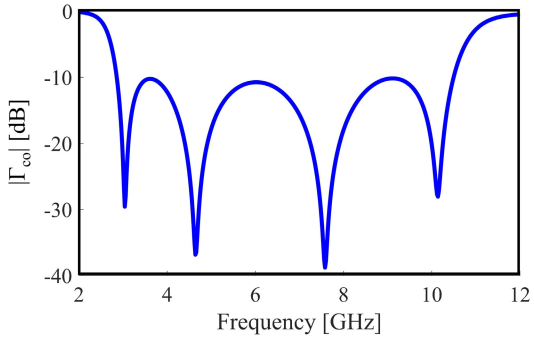

FIGURE 6. The reflection coefficient (equivalent to RCS reduction) of the structure of FIGURE 1, which is theoretically obtained using (7).

simulation of the entire structure; instead, it was analytically computed by assuming that each of the four arrays of the overall structure is infinite. Based on the theoretical results, an RCS reduction of more than 10 dB is achieved in the frequency range of 2.85 GHz to 10.49 GHz (i.e., FBW = 115%), as shown in FIGURE 6. It is noticeable that in our work, similar to other phase cancellation and polarization conversion methods, the RCS reduction is due to redirecting the incident wave, not absorbing it. Our simulation results show that changing the loss tangent of the substrate does not impact the RCS reduction considerably.

It should be noted that using the polarization conversion technique [13], [14], [15], [16], [17], [18], the RCS reduction is only achieved in the frequency range where the unit cell (in a periodic array) rotates the polarization of the incident wave

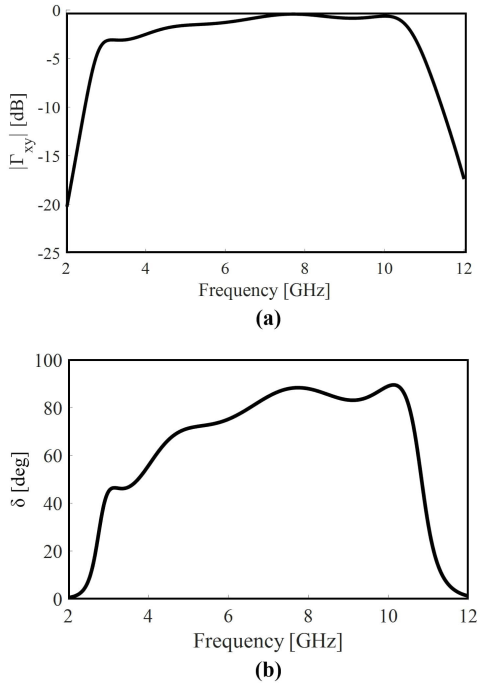

FIGURE 7. (a) $|\Gamma_{xy}|$ and (b) the polarization rotation angle (δ) of a periodic array of the unit cell illustrated in FIGURE 4.

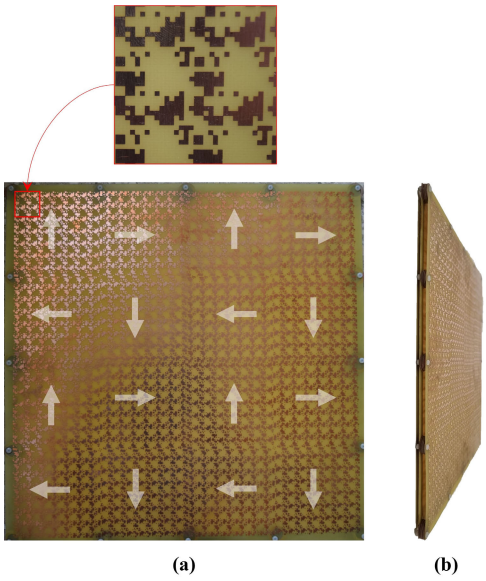

FIGURE 8. The fabricated RCS reducer comprising of 2 × 2 building blocks shown in FIGURE 9 (4 × 4 rotated arrays of the unit cell shown in FIGURE 4): (a) top view and (b) side view.

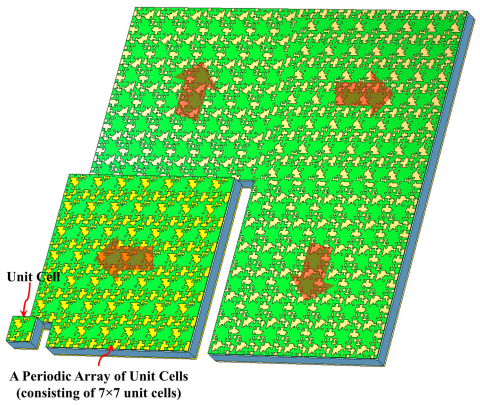

FIGURE 9. A building block of the fabricated RCS reducer surface composed of 2 × 2 rotated arrays of the unit cell. Each array within the building block is made up of 7 × 7 optimized unit cells.

90 degrees. However, FIGURE 5(a) shows that using the proposed method, for frequencies lower than 6 GHz, although RCS reduction is achieved (as shown in FIGURE 6), Γ_{yy} (and also Γ_{xx}) has a larger value than -10 dB, indicating that the wave polarization is not rotated 90-degrees. In order to demonstrate the polarization rotation by the pattern optimized unit cell more clearly, Γ_{xy} is shown in FIGURE 7(a), and the polarization rotation angle (i.e., the angle between the polarization vectors of reflected wave and incident wave) from a periodic array of the unit cell is calculated as

$$\delta = \tan^{-1}\left|\frac{\Gamma_{xy}}{\Gamma_{yy}}\right| \tag{12}$$

which is depicted in FIGURE 7(b). As can be seen in this figure, in the frequency range of 2.85 GHz to 10.49 GHz, where the RCS reduction is greater than 10 dB, the polarization rotation angle varies between 35 and 90 degrees.

IV. VALIDATION

To ensure precise measurement, a prototype comprising of 2 × 2 building blocks with an overall size of around 45 cm × 45 cm, corresponding to 3λ × 3λ at the lowest frequency of interest, 2 GHz, was fabricated as shown in FIGURE 8. The building block of the fabricated RCS reducer consisting of 2 × 2 arrays, rotated relative to each other, and each of them is comprised of 7 × 7 of the optimized unit cells shown in FIGURE 4 is also depicted in FIGURE 9. It is worth mentioning that the arrays have to be large enough to contain at least four periods of the unit cell to ensure that the behavior (reflection phase) of the periodic structure is obtained [3]. It is also noticeable that the arrays are positioned precisely adjacent to each other. To form the air gap between the substrate and the ground plate, Teflon spacers were utilized at the board edges. The monostatic RCS reduction compared to a same-sized metal plate under a normal incidence was determined in an anechoic chamber, as shown in FIGURE 10, and the result is shown in FIGURE 11. According to the measurement result, in the frequency range of 2.8 GHz to 10.4 GHz, an RCS reduction of better than 10 dB has been achieved. It can also be observed that the results obtained by experimental measurements, full-wave simulation of the building block shown in FIGURE 9, and the proposed theory (using Eq. (7)) exhibit a good degree of agreement,

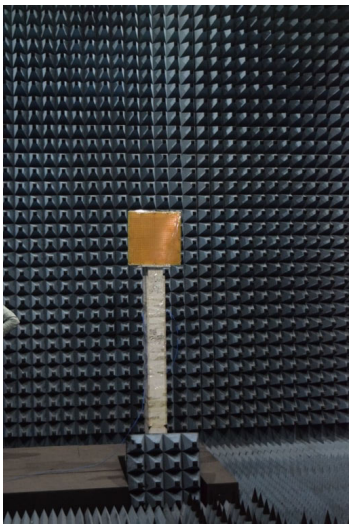

FIGURE 10. The measurement setup in an anechoic chamber.

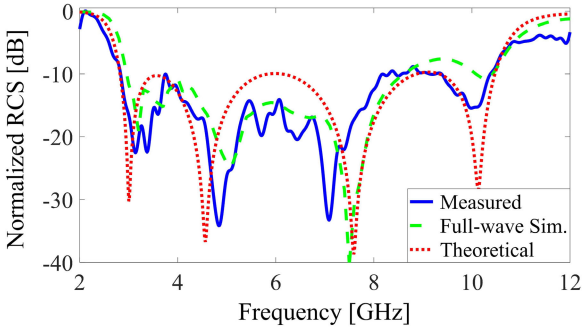

FIGURE 11. Normalized monostatic RCS of the fabricated surface (relative to an equal size metallic plate) obtained by measurements, full-wave simulation of the structure shown in FIGURE 9, and proposed theory using (7).

validating the generalized phase-polarization cancellation method proposed in this work. It is worth noting that the measurements were conducted on a prototype consisting of 2×2 building blocks (which translates to 4×4 arrays of the unit cell); however, for the purpose of reducing computation costs, the full-wave simulation was carried out for a single building block comprising of 2×2 arrays.

The simulated 3-D pattern of the scattered field from the RCS reducer surface is illustrated in FIGURE 12(a) at the frequency corresponding to the maximum RCS reduction (7.7 GHz). In comparison, FIGURE 12(b) shows the scattered field pattern from a PEC plate of identical size. It is evident that the PEC plate predominantly reflects the energy towards the incident direction ($z-$direction), while the designed surface redirects the incident waves into four diagonal lobes. This redirection significantly reduces reflection in the z-direction, thereby effectively achieving the desired mono-static RCS reduction.

To investigate the angular stability of the designed RCS reducer surface, full-wave simulations were employed instead of measurements due to the infeasibility of measuring

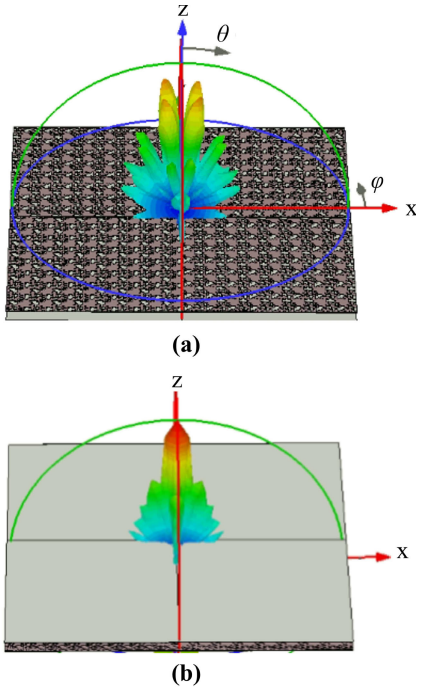

FIGURE 12. 3-D pattern of scattered field from (a) the designed RCS reducer surface and (b) a PEC plate with the same size at 7.7 GHz.

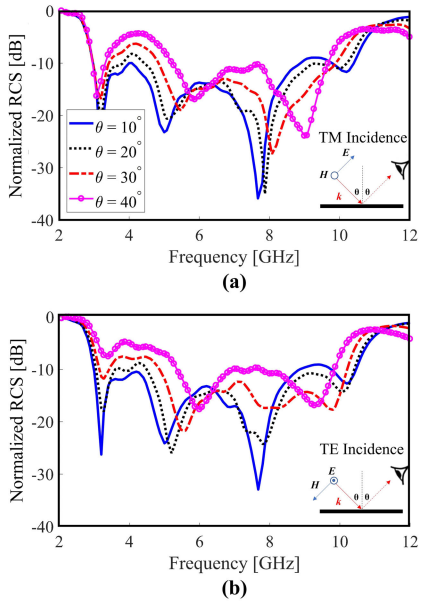

FIGURE 13. Simulated bistatic RCS of the designed RCS reducer surface (normalized with respect to an equal size metallic plate) under oblique (a) TM and (b) TE incidences.

RCS under oblique incidence in the chamber. FIGURE 13 illustrates the results for TM and TE incidences at angles ranging from 10 to 40 degrees. It is observed that increasing the incident angle reduces the performance of the RCS reduction, particularly for TE incidence, as the unit cell was designed under the assumption of normal incidence. However, this is not a unique challenge for our design; it is

TABLE 1. Comparison between RCS reducer surfaces employing phase cancellation and polarization conversion methods.

Reference / Years	RCS Reduction Method	Type of Surface	10-dB monostatic RCS Reduction Bandwidth [GHz]	Fractional Bandwidth [%]	Substrate's height [mm] (dielectric constant)
[3] 2013	Phase cancellation	Checkerboard (including two types of AMC cells)	14.4–21.8	41	1.3 (10.2)
[4] 2013			9–15	50	3.3 (2.2)
[2] 2009			13.2–24.2	58	1.6 (2.5)
[10] 2019			8-16.3	69	3.2 (2.2)
[8] 2018			5.4-14.2	90	0.8 (3.7) + 3.6 (1)
[9] 2019			3.8 - 10.1	91.5	0.5 (3.5) + 11 (1)
[7] 2017			3.8-10.7	95	0.8 (3.38) + 6 (2.2)
[12] 2021			4.9–14.3	98	1.6 (2.3) + 5 (1)
[11] 2021			4.1-12.3	100	1.6 (4.3) + 5 (1)
[17] 2022	Polarization conversion	Four rotated arrays of a single AMC cell	8.1-14.6	57	2 (9.7)
[15] 2020			8.8-20.9	82	3 (2.7)
[13] 2016			6.0-18.0	100	3 (4.4)
[16] 2020			5-15	100	0.3 (4.3) + 2.5 (1)
[18] 2022			9.5-32.5	109	0.2 (2.7) + 2.8 (1)
This work	Generalized phase -polarization cancellation		2.8-10.4	115	0.5 (4.3) + 7.6 (1)

also a limitation for other designs reported in the literature [1], [2], [3], [4], [5], [6], [7], [8], [9], [10], [11], [12], [13], [14], [15], [16], [17], [18].

Finally, in TABLE 1, a comparison is made between RCS reducer surfaces designed using the phase cancellation, polarization conversion, and generalized phase-polarization cancellation methods. As indicated in this table, two types of symmetric AMC unit cells are used in the RCS reducer surfaces designed based on phase cancellation; however, those designed using the polarization conversion method and the proposed method consist of rotated arrays of only one unit cell. It can be seen the 10-dB RCS reduction bandwidth in this article is competitive with the state-of-the-art RCS reducers. The table also compares the substrates' height (and dielectric constant) used in different works. It is noticeable the minimum operating frequency in our work is considerably lower than all other works (ours is 2.8 GHz, while the second lowest is 3.8 GHz); however, the height of our RCS reducer surface is not that different from other works with relatively similar frequency bands [7], [9], [11], [12].

V. CONCLUSION

In this study, a novel approach for reducing RCS was developed by combining the phase cancellation and polarization conversion methods. The proposed approach employs arrays of a unit cell, each of which is rotated 90 degrees relative to its neighboring arrays, to form an RCS reducer surface. Due to the lack of symmetry in the unit cell, each array can arbitrarily rotate the polarization of the incident wave. However, as the arrays are arranged in a rotational symmetry, the reflected wave from the whole surface is co-polarized with the incident wave. Analytical derivations were carried out to derive the RCS reduction condition for the overall structure (composed of four rotated arrays).

A pattern optimization approach based on pixelization of the unit cell's surface and the binary particle swarm optimization (BPSO) algorithm was employed to design a unit cell that satisfies the RCS reduction criterion at the greatest achievable bandwidth. By implementing the designed unit cell in the proposed structure (four rotated arrays), a 10-dB monostatic RCS reduction from 2.85 GHz to 10.49 GHz was theoretically achieved. A surface was built by patterning 4×4 arrays of 7×7 designed unit cells, each of which was rotated 90 degrees relative to its side arrays. The measurement results showed a 10-dB monostatic RCS reduction bandwidth of 2.8 GHz to 10.4 GHz (a FBW of 115%) was reached, which is in good accordance with the theoretical result. The angular stability of the RCS reducer surface under oblique TE and TM incidences was examined using full-wave simulations. Good angular stability was observed. Finally, compared to earlier works employing phase cancellation and polarization conversion approaches, a broader RCS reduction bandwidth was achieved using the proposed generalized method.

ACKNOWLEDGMENT

(Mohammad Shirmohammadkarimi and Ali Ghadimi contributed equally to this work.)

REFERENCES

[1] M. Paquay, J.-C. Iriarte, I. Ederra, R. Gonzalo, and P. de Maagt, "Thin AMC structure for radar cross-section reduction," *IEEE Trans. Antennas Propag.*, vol. 55, no. 12, pp. 3630–3638, Dec. 2007.

[2] Y. Zhang, R. Mittra, B. Z. Wang, and H. T. Huang, "AMCs for ultra-thin and broadband RAM design," *Electron. Lett.*, vol. 45, no. 10, pp. 484–485, 2013.

[3] J. C. I. Galarregui, A. T. Pereda, J. L. M. de Falcón, I. Ederra, R. Gonzalo, and P. de Maagt, "Broadband radar cross-section reduction using AMC technology," *IEEE Trans. Antennas Propag.*, vol. 61, no. 12, pp. 6136–6143, Dec. 2013.
[4] A. Edalati and K. Sarabandi, "Wideband, wide angle, polarization independent RCS reduction using nonabsorptive miniaturized-element frequency selective surfaces," *IEEE Trans. Antennas Propag.*, vol. 62, no. 2, pp. 747–754, Feb. 2014.
[5] W. Chen, C. A. Balanis, and C. R. Birtcher, "Checkerboard EBG surfaces for wideband radar cross section reduction," *IEEE Trans. Antennas Propag.*, vol. 63, no. 6, pp. 2636–2645, Jun. 2015.
[6] W. Chen, C. A. Balanis, and C. R. Birtcher, "Dual wide-band checkerboard surfaces for radar cross section reduction," *IEEE Trans. Antennas Propag.*, vol. 64, no. 9, pp. 4133–4138, Sep. 2016.
[7] M.-J. Haji-Ahmadi, V. Nayyeri, M. Soleimani, and O. M. Ramahi, "Pixelated checkerboard metasurface for ultra-wideband radar cross section reduction," *Sci. Rep.*, vol. 7, no. 1, pp. 1–12, Sep. 2017.
[8] J. Xue, W. Jiang, and S. Gong, "Chessboard AMC surface based on quasi-fractal structure for wideband RCS reduction," *IEEE Antennas Wireless Propag. Lett.*, vol. 17, no. 2, pp. 201–204, Feb. 2018.
[9] D. Sang, Q. Chen, L. Ding, M. Guo, and Y. Fu, "Design of checkerboard AMC structure for wideband RCS reduction," *IEEE Trans. Antennas Propag.*, vol. 67, no. 4, pp. 2604–2612, Apr. 2019.
[10] S. H. Kim and Y. J. Yoon, "Wideband radar cross-section reduction on checkerboard metasurfaces with surface wave suppression," *IEEE Antennas Wireless Propag. Lett.*, vol. 18, no. 5, pp. 896–900, May 2019.
[11] A. Murugesan, D. Natarajan, and K. T. Selvan, "Low-cost, wideband checkerboard metasurfaces for monostatic RCS reduction," *IEEE Antennas Wireless Propag. Lett.*, vol. 20, no. 4, pp. 493–497, Apr. 2021.
[12] A. Murugesan and K. T. Selvan, "On further enhancing the bandwidth of wideband RCS reduction checkerboard metasurfaces using an optimization algorithm," *Int. J. RF Microw. Comput.-Aided Eng.*, vol. 31, no. 7, Jul. 2021, Art. no. e22686.
[13] Y. Liu, K. Li, Y. Jia, Y. Hao, S. Gong, and Y. J. Guo, "Wideband RCS reduction of a slot array antenna using polarization conversion metasurfaces," *IEEE Trans. Antennas Propag.*, vol. 64, no. 1, pp. 326–331, Jan. 2016.
[14] C. Fu, L. Han, C. Liu, Z. Sun, and X. Lu, "Dual-band polarization conversion metasurface for RCS reduction," *IEEE Trans. Antennas Propag.*, vol. 69, no. 5, pp. 3044–3049, May 2021.
[15] M. Zhang, X. Yang, J. Luo, T. Zhou, Z. Li, X. Lei, and J. Chen, "A polarization conversion coding metasurface for broadband radar cross-section reduction," *J. Electron. Mater.*, vol. 49, no. 9, pp. 5561–5569, Sep. 2020.
[16] A. Oruji, A. Pesarakloo, and M. Khalaj-Amirhosseini, "Ultrawideband and omnidirectional RCS reduction by using symmetrical coded structures," *IEEE Antennas Wireless Propag. Lett.*, vol. 19, no. 7, pp. 1236–1240, Jul. 2020.
[17] T. Han, K. Wen, Z. Xie, and X. Yue, "An ultra-thin wideband reflection reduction metasurface based on polarization conversion," *Prog. Electromagn. Res.*, vol. 173, pp. 1–8, 2022.
[18] J. Liu, J.-Y. Li, and Z. N. Chen, "Broadband polarization conversion metasurface for antenna RCS reduction," *IEEE Trans. Antennas Propag.*, vol. 70, no. 5, pp. 3834–3839, May 2022.
[19] P. Su, Y. Zhao, S. Jia, W. Shi, and H. Wang, "An ultra-wideband and polarization-independent metasurface for RCS reduction," *Sci. Rep.*, vol. 6, no. 1, pp. 1–8, Feb. 2016.
[20] X. Liu, J. Gao, L. Xu, X. Cao, Y. Zhao, and S. Li, "A coding diffuse metasurface for RCS reduction," *IEEE Antennas Wireless Propag. Lett.*, vol. 16, pp. 724–727, 2017.
[21] X. Han, H. Xu, Y. Chang, M. Lin, Z. Wenyuan, X. Wu, and X. Wei, "Multiple diffuse coding metasurface of independent polarization for RCS reduction," *IEEE Access*, vol. 8, pp. 162313–162321, 2020.
[22] Z. Ren, Y.-Q. Liu, Y. Wang, L. Lu, K. Qi, and H. Yin, "Ultra-broadband RCS reduction based on optimized coding 'whale-shaped' polarization conversion metasurface with angular stability," *IEEE Access*, vol. 10, pp. 50479–50486, 2022.
[23] A. Ghadimi, M. Shirmohammadkarimi, M. Soleimani, and V. Nayyeri, "Broadband radar cross section reduction using generalized phase-polarization cancellation," in *Proc. 52nd Eur. Microw. Conf. (EuMC)*, Sep. 2022, pp. 728–731.
[24] H. Shan, K. Jiang, J. Xing, and T. Jiang, "BPSO and staggered triangle layout optimization for wideband RCS reduction of pixelate checkerboard metasurface," *IEEE Trans. Microw. Theory Techn.*, vol. 70, no. 7, pp. 3406–3414, Jul. 2022.
[25] D. J. Kern, D. H. Werner, A. Monorchio, L. Lanuzza, and M. J. Wilhelm, "The design synthesis of multiband artificial magnetic conductors using high impedance frequency selective surfaces," *IEEE Trans. Antennas Propag.*, vol. 53, no. 1, pp. 8–17, Jan. 2005.
[26] Z. Bayraktar, M. D. Gregory, X. Wang, and D. H. Werner, "A versatile design strategy for thin composite planar double-sided high-impedance surfaces," *IEEE Trans. Antennas Propag.*, vol. 60, no. 6, pp. 2770–2780, Jun. 2012.
[27] B. Ghaderi, V. Nayyeri, M. Soleimani, and O. M. Ramahi, "Pixelated metasurface for dual-band and multi-polarization electromagnetic energy harvesting," *Sci. Rep.*, vol. 8, no. 1, pp. 1–12, Sep. 2018.
[28] A. Ghadimi, V. Nayyeri, M. Khanjarian, M. Soleimani, and O. M. Ramahi, "Design and simulation of a wideband, wide-angle and polarization-insensitive microwave absorber based on pattern optimization of resistive films," *J. Phys. D, Appl. Phys.*, vol. 54, no. 5, Feb. 2021, Art. no. 055102.
[29] M. Saadat-Safa, V. Nayyeri, A. Ghadimi, M. Soleimani, and O. M. Ramahi, "A pixelated microwave near-field sensor for precise characterization of dielectric materials," *Sci. Rep.*, vol. 9, no. 1, pp. 1–12, Sep. 2019.
[30] A. Ghadimi, V. Nayyeri, M. Khanjarian, M. Soleimani, and O. M. Ramahi, "A systematic approach for mutual coupling reduction between microstrip antennas using pixelization and binary optimization," *IEEE Antennas Wireless Propag. Lett.*, vol. 19, no. 12, pp. 2048–2052, Dec. 2020.
[31] M. Borgese, F. Costa, S. Genovesi, A. Monorchio, and G. Manara, "Optimal design of miniaturized reflecting metasurfaces for ultra-wideband and angularly stable polarization conversion," *Sci. Rep.*, vol. 8, no. 1, pp. 1–11, May 2018.
[32] A. Hojjati, M. Soleimani, V. Nayyeri, and O. M. Ramahi, "Ternary optimization for designing metasurfaces," *Sci. Rep.*, vol. 11, no. 1, pp. 1–9, Aug. 2021.
[33] S. Genovesi, R. Mittra, A. Monorchio, and G. Manara, "Particle swarm optimization for the design of frequency selective surfaces," *IEEE Antennas Wireless Propag. Lett.*, vol. 5, pp. 277–279, 2006.
[34] R. Eberhart and J. Kennedy, "A new optimizer using particle swarm theory," in *Proc. MHS. Proc. 6th Int. Symp. Micro Mach. Human Sci.*, Oct. 1995, pp. 39–43.
[35] N. Jin and Y. Rahmat-Samii, "Advances in particle swarm optimization for antenna designs: Real-number, binary, single-objective and multiobjective implementations," *IEEE Trans. Antennas Propag.*, vol. 55, no. 3, pp. 556–567, Mar. 2007.
[36] R. Poli, J. Kennedy, and T. Blackwell, "Particle swarm optimization," *Swarm Intell.*, vol. 1, no. 1, pp. 33–57, Jun. 2007.
[37] X. Jun and H. Chang, "The discrete binary version of the improved particle swarm optimization algorithm," in *Proc. Int. Conf. Manage. Service Sci.*, Sep. 2009, pp. 1–6.
[38] A. P. Engelbrecht, *Fundamentals of Computational Swarm Intelligence*. Hoboken, NJ, USA: Wiley, 2006.

MOHAMMAD SHIRMOHAMMADKARIMI was born in Damavand, Tehran, Iran, in 1993. He received the B.Sc. degree in electrical engineering from the University of Semnan, in 2017, and the M.Sc. degree in electrical engineering from the Iran University of Science and Technology (IUST), Tehran, in 2020, where he is currently pursuing the Ph.D. degree in electrical engineering. His research interests include antennas, metamaterials, metasurfaces, and electromagnetic wave propagation.

ALI GHADIMI was born in 1993. He received the master's degree in satellite engineering (satellite communication) from the Iran University of Science and Technology in 2019. He is a dedicated researcher in the field of electrical engineering, specializing in antennas, metamaterials, and applied electromagnetics.

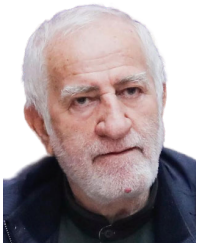

MOHAMMAD SOLEIMANI received the B.Sc. degree in electrical engineering from the University of Shiraz, Shiraz, Iran, in 1978, and the M.Sc. and Ph.D. degrees from Pierre and Marie Curio University, Paris, France, in 1981 and 1983, respectively. He is currently a Professor with the School of Electrical Engineering, Iran University of Sciences and Technology, Tehran, Iran, and the Director of the Antenna and Microwave Research Laboratory. He also has several executive and research positions. He has authored and coauthored 19 books (in Persian) and over 200 journal and conference papers. His research interests include electromagnetics, high-frequency electronics, and antennas.

VAHID NAYYERI (Senior Member, IEEE) received the B.Sc. degree from the Iran University of Science and Technology (IUST), Tehran, Iran, in 2006, the M.Sc. degree from the University of Tehran, Tehran, in 2008, and the Ph.D. degree from IUST, in 2013, all in electrical engineering.

From 2007 to 2013, he was a Research Assistant with IUST and then a Visiting Scholar with the University of Waterloo, ON, Canada. In 2013, he joined the Faculty of IUST, where he is currently an Associate Professor, the Director of the Advanced Radio Circuits and Systems Laboratory, and the Head of the Department of Satellite Technology. In 2019, he was a Visiting Professor with the University of Waterloo. He has authored and coauthored one book (in Persian) and over 110 technical articles. His research interests include applied and computational electromagnetics and microwave active and passive circuits.

Dr. Nayyeri received the Best Ph.D. Thesis Award from the IEEE Iran Section, in 2014. He serves on the IEEE Iran Section as a member of the Board of Directors, the Chair of the Membership Development Committee, and a Steering Committee Member of the Electromagnetics and Photonics Chapter. He was a Guest Editor of two special issues of *Sensors*, in 2019 and 2020. He serves as an Associate Editor for the IEEE TRANSACTIONS ON MICROWAVES THEORY TECHNIQUES and the *IET Microwaves, Antennas, and Propagation*.